Theoretical Investigation of the Electronic Structure of the Mixed-Sandwich Complex (η^5-Cyclopentadienyl)(η^6-benzene)iron and Its Cation

A. Le Beuze,*,† R. Lissillour,† and J. Weber‡

Laboratoire de Chimie Théorique, UA CNRS 1495, Université de Rennes I, Avenue du General Leclerc, 35042 Rennes Cedex, France, and Département de Chimie Physique, Université de Genève, 30 quai Ernest-Ansermet, 1211 Genève 4, Switzerland

Received January 21, 1992

SCF MS–Xα calculations have been carried out for the d^6 $[(Cp)Fe(Bz)]^+$ (**1**) and d^7 (Cp)Fe(Bz) (**2**) compounds (Cp = η^5-cyclopentadienyl, Bz = η^6-benzene), and the results are compared with those previously reported for metallocenes $Fe(Cp)_2$ (**3**), $Co(Cp)_2$ (**4**), $[Ni(Cp)_2]^+$ (**5**), and d^8 $Ni(Cp)_2$ (**6**) using the same technique. Analysis of the electronic structure of **1** and **2** shows that whereas Cp and Bz ligands play roughly the same role in π-ligand to metal donation, they behave differently as far as 3dδ back-donation is concerned, the Bz system having a much more important role in this case. This is confirmed by spin-polarized (SP) calculations performed for **2** and **4**, which show that the 3dδ orbitals exhibit a much larger interaction with the Bz ligand than with the Cp group. In addition, a considerable charge relaxation occurs at the metal upon ionization of **2**, as the gross charges on the iron are roughly the same in **1** and **2**. When using the MS–Xα results to calculate spectroscopic properties, a good agreement is found between theoretical and experimental results determined for both the electron field gradient (EFG) at the metal nucleus and Mössbauer isomer shift (IS) for compounds **1–3**. Similarly, both MS–Xα ionization and electronic excitation energies calculated for **1** and **2** compare fairly well with photoelectron and UV–visible absorption data.

I. Introduction

The electronic structures of metallocene and bis(arene) sandwich complexes have been the subject of numerous theoretical investigations by means of ligand field, semiempirical, and the more sophisiticated SCF ab initio and Xα methods.[1] The results of these studies have been, in general, directly compared with spectroscopic data, which has largely contributed to a better understanding of the chemical bonding in these complexes. In contrast to these symmetric bis(benzene) and bis(cyclopentadienyl) complexes, few papers have been published concerning the electronic structure of dissymmetric mixed-sandwich species.[2]

A simple prototype of dissymmetric mixed sandwiches can be found in the 19e⁻ (Cp)Fe(Bz) complex, a reduced form of a stable and totally reversible system (Scheme I) exhibiting a high redox potential.[3] As several experimental studies[3] have been performed for this series of compounds, it was of interest to carry out a theoretical investigation

Scheme I

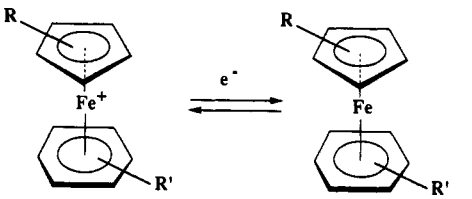

1 Fe(II) **2** Fe(I)

using the SCF MS–Xα model. Indeed, the study of such transition-metal complexes has turned out to be an ideal field for the application of the MS–Xα method.[1d,i,j,4] As detailed Xα calculations have been carried out for the d^6 ferrocene,[1d] d^7 cobaltocene,[1j] and d^8 nickelocene and its cation,[1i] it was therefore of interest to perform similar calculations on the d^6 and d^7 Cp/Bz (Cp = η^5-cyclopentadienyl; Bz = η^6-benzene) mixed compounds in order to extend the theoretical information to these homogeneous series of compounds.

The main purpose of the present work is to provide a realistic description of the electronic structure of the 19-

† Université de Rennes I.
‡ Université de Genève.

(1) (a) Prins, R. *Mol. Phys.* **1970**, *19*, 603. (b) Aderson, S. E.; Drago, R. *Inorg. Chem.* **1972**, *11*, 1664. (c) Coutière, M. M.; Demuynck, J.; Veillard, A. *Theor. Chim. Acta* **1972**, *27*, 281. (d) Rösch, N.; Johnson, K. H. *Chem. Phys. Lett.* **1974**, *24*, 179. (e) Botrel, A.; Dibout, P.; Lissillour, R. *Theor. Chim. Acta* **1975**, *37*, 37. (f) Bagus, P. S.; Walgren, U. I.; Almlof, J. *J. Chem. Phys.* **1976**, *64*, 2324. (g) Lissillour, R. *J. Chim. Phys.* **1979**, *76*, 1103. (h) Haaland, A. *Acc. Chem. Res.* **1979**, *12*, 415. (i) Goursot, A.; Penigault, E.; Ammeter, J. H.; Backman, J. *J. Am. Chem. Soc.* **1982**, *104*, 1491. (k) Rösch, N.; Streitwieser, A., Jr.; *J. Am. Chem. Soc.* **1983**, *105*, 7237.

(2) (a) Clack, D. W.; Warren, K. D. *J. Organomet. Chem.* **1978**, *152*, C60. (b) Mariot, J. P.; Michaud, P.; Iauer, S.; Astruc, D.; Trautwein, A. X.; Varet, F. *J. Phys.* **1983**, *44*, 1377. (c) Lacoste, M.; Rabaa, H.; Astruc, D.; Le Beuze, A.; Saillard, J. Y.; Precigoux, G.; Courseille, C.; Ardouin, N.; Bowyer, W. *Organometallics* **1989**, *8*, 2233.

(3) (a) Astruc, D. *Acc. Chem. Res.* **1986**, *19*, 377. (b) Astruc, D. *Chem. Rev.* **1988**, *88*, 1189 and references therein.

(4) (a) Case, D. A.; Karplus, M. *J. Am. Chem. Soc.* **1977**, *99*, 6132. (b) Case, D. A.; Huynh, B. H.; Karplus, M. *J. Am. Chem. Soc.* **1979**, *101*, 433. (c) Norman, J. R., Jr.; Renzoni, G. E.; Case, D. A. *J. Am. Chem. Soc.* **1979**, *101*, 5265. (d) Lie, S. K.; Taft, C. A. *Chem. Phys. Lett.* **1982**, *89*, 463. (e) Sunil, K. K.; Harrisson, J. F.; Rogers, M. *J. Chem. Phys.* **1982**, *76*, 3078. (f) Bencini, A.; Gatteschi, D. *J. Am. Chem. Soc.* **1983**, *105*, 5535. (g) Maroney, M. J.; Norman, J. G., Jr.; Osborne, H. *Inorg. Chem.* **1984**, *23*, 2261. (h) Perfield, K. W.; Gewith, A. A.; Solomon, E. I. *J. Am. Chem. Soc.* **1985**, *107*, 4519. (i) Noodleman, L.; Norman, J. G., Jr.; Osborne, H.; Aizman, A.; Case, D. A. *J. Am. Chem. Soc.* **1985**, *107*, 3418. (j) Goursot, A.; Chermette, H.; Chanon, M.; Waltz, W. L. *Inorg. Chem.* **1985**, *24*, 1042. (k) Weber, J.; Kündig, E. P.; Goursot, A.; Penigault, E. *Can. J. Chem.* **1985**, *63*, 1734. (l) Bencini, A.; Gatteschi, D. *J. Am. Chem. Soc.* **1986**, *108*, 5763. (m) Weber, J.; Chermette, H.; Heck, J.; *Organometallics* **1989**, *8*, 2544. (n) Applications of the Density Functional to the Properties of Inorganic Systems. Presented at a symposium in Arles, France, Sept 27, 1988; *J. Chim. Phys.* **1989**, *86* (4).

0276-7333/93/2312-0047$04.00/0

Scheme II

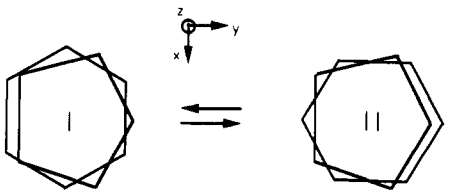

electron mixed sandwich (Cp)Fe(Bz) (d^7) and its cation (d^6). First, we shall describe the main features of the chemical bonding in $[(Cp)Fe(Bz)]^+$ (1) and (Cp)Fe(Bz) (2) and then compare them with those of their d^6, d^7, and d^8 symmetric analogues, namely $Fe(Cp)_2$ (3), $Co(Cp)_2$ (4), $[Ni(Cp)_2]^+$ (5), and $Ni(Cp)_2$ (6). Then, polarization effects of the unpaired electron on bonding in 2 and 4 will be discussed. Moreover, these calculations should give additional information with regard to the total s-electron densities at the nucleus in order to analyze the electronic hyperfine parameters and directly compare with Mössbauer results. Finally, theoretical results concerning ionization and electronic excitation energies of 1 and 2 will be compared with experimental data such as photoelectron[5] and UV–visible absorption[6] spectroscopy.

II. Computational Details

The standard version of the density functional SCF MS–Xα method[7] is used and applied to complexes 1 and 2. It is well-known that this model is based on the local Hartree–Fock–Slater Hamiltonian,[8a] whose eigensolutions are found by using the multiple-scattering (or scattered-wave (SW)) approximation.[7] The method has been described in detail in several articles,[7,8] and it does not need further development here. However, some computational details as well as the choice of the calculation parameter deserve comment.

A standard C_s symmetry is assumed for the complexes, using planar ligand rings and standard C–C (1.40 Å) and C–H (1.10 Å) bond lengths. The metal distances Fe–Cp = 1.78 Å and Fe–Bz = 1.54 Å for the radical complex and Fe^+–Cp = 1.68 Å and Fe^+–Bz = 1.55 Å for the cation have been taken from structural data available for related substituted compounds.[9] In the C_s symmetry (i.e. the yz plane being the mirror plane), the two conformations I and II are possible, differing in rotation of the Bz ring by 90° (see Scheme II). Calculations have been carried out for these two conformations.

The radii of muffin-tin spheres, characteristic of the MS–Xα model, were chosen as follows: starting from geometry-induced touching spheres, obtained for metal and ligand atoms, the carbon radii were enlarged by 25% to provide a better description of the ring systems and an additional empty sphere (E) was located in the center of each ligand ring. This procedure, which has been shown[10j] to give reliable results for similar complexes, leads to the muffin-tin radii (au) r(Fe) = 2.2795, r(C) = 1.6535, r(H) = 0.8758, r(E-Bz) = 1.3226, and r(E–Cp) = 1.0843. Finally, the radii of the outer spheres (r(OUT)) of the complexes 2 and 1 are 6.4246 and 6.4336 au, respectively.

The exchange scaling parameters α were taken from the tabulation of Schwarz[10a] for Fe (0.711 51) and C (0.753 31) and from an article by Slater[10b] for H (0.777 25). The α parameters of the empty spheres and the outer sphere (α(E-Bz) = α(E-Cp) = α(OUT) = 0.762 90) are obtained from the weighted average of the atomic values. The maximum L values in the partial wave expansion included in the calculation were L = 2 in the metal sphere, L = 1 for carbon and empty spheres, L = 0 for hydrogen spheres, and L = 3 in the extramolecular region. For the cation, a Watson sphere,[11] having the same radius as the outer sphere and bearing the charge −1, has been introduced in order to mimic the external stabilizing electrostatic field. The transition-state method[12] has been used to calculate ionization and excitation energies.

III. Results and Discussion

A. Electronic Structure and Chemical Bonding. (i) The Mixed (Cp)Fe(Bz) Radical 2. Non-spin-polarized (NSP) energy levels and charge distributions are presented in Table I for this radical in conformation I, and the corresponding molecular orbital (MO) diagram is depicted in Figure 1. The sequence of MO's with predominant Fe 3d character is $18a'(x^2 - y^2)$, $12a''(xy)$ $[3d\delta^4]$ < $19a'(z^2)$ $[3d\sigma^2]$ ≪ $20a'(yz)$, $13a''(xz)$ $[3d\pi^1]$, in accordance with the order for the related metallocene compounds, $e_{2g} < a_{1g} \ll e_{1g}$.[1]

The highest occupied MO, containing the unpaired electron, has about 66% Fe 3d character and displays a strong antibonding interaction, primarily with the π-Cp ligand (14%) and in a lesser part with the π-Bz group (6%). The 2A″(I) ground state of conformer I is characterized by occupation of the 13a″ MO by the unpaired electron, though the unoccupied 20a′ MO is found at slightly lower energy. For conformer II the 2A′(II) ground state corresponds to the reverse order $13a''^0 < 20\ a'^1$.

It is usual to describe the chemical bonding in such sandwich complexes by means of a synergic effect: a π ligand-to-metal 3d donation versus a π back-bonding from the metal 3d orbitals to the π ligand orbitals, the 4s and 4p orbitals of metal being involved to a smaller extent in this mechanism.

a. π-Ligand Donation to the Fe 3d Subshell. Clearly, the amount of this charge donation may be deduced from Fe 3d participation in corresponding bonding ligand–metal MO's. Thus, most of the covalent ligand–metal interaction occurs through the two sets of paired MO's (9a″, 16a′) and (17a′, 11a″). As shown in Scheme III, where the main orbital interactions between 3d metal orbitals and π-ligand MO's are displayed, they correspond actually to the stabilized e_{1g} and e''_1 π MO's of C_6H_6 and C_5H_5, respectively. Their strongly bonding character, which shows a significant π-ligand → Fe donation, is underlined in Figure 2a, which displays the contour maps of the 9a″ and 17a′ MO's. A fair amount of the Fe 3d population arises, for the most part, from the Cp ligand electrons (i.e. 17% of Fe 3d character in the π-Cp orbital versus 10% in the π-Bz ones). This is due to a smaller energy difference between the $1e''_1$ MO of C_5H_5 and the Fe 3d atomic level as compared with Bz levels. Indeed, π levels of the ligand are gradually stabilized when the ligand size increases (i.e. increasing the number of carbon atoms in the ring).

b. π Back-Bonding. In metallocene (d^6) compounds, the π back-bonding essentially occurs through the δ *back-donation* from the 3dδ orbitals of the metal to the π^* unoccupied ligand MO's. This phenomenon occurs again

(5) Green, J. C.; Kelly, M. R.; Payne, M. P.; Seydon, E. A.; Astruc, D.; Hamon, J. R.; Michaud, P. *Organometallics* **1983**, *2*, 211.
(6) Astruc, D.; Hamon, J. R.; Althoff, G.; Roman, E.; Batail, P.; Michaud, P.; Mariot, J. P.; Varret, F.; Cozak, D. *J. Am. Chem. Soc.* **1979**, *101*, 5445.
(7) Johnson, K. H. *Adv. Quantum Chem.* **1973**, *7*, 143.
(8) (a) Slater, J. C. *Quantum Theory of Molecules and Solids*; McGraw-Hill: New York, 1974. (b) Danese, J. B.; Connoly, J. W. D. *J. Chem. Phys.* **1974**, *61*, 3063.
(9) Hamon, J. R.; Astruc, D.; Roman, E.; Batail, P.; Mayerle, J. J. *J. Am. Chem. Soc.* **1983**, *103*, 2431.
(10) (a) Schwarz, K. *Phys. Rev.* **1972**, *B6*, 2466. (b) Slater, J. C. *Int. J. Quantum Chem., Quantum Chem. Symp.* **1973**, *7*, 533.
(11) Watson, R. E. *Phys. Rev.* **1958**, *111*, 1108.
(12) Slater, J. C. *Adv. Quantum Chem.* **1972**, *6*, 1.

Table I. Spin-Restricted SW-Xα Upper Valence Levels and Charge Distributions[a]

			Fe		Cp		Bz					
orbital	occ (e⁻)	energy (eV)	% p	% d	% pσ	% pπ	% s	% pσ	% pπ	% H	% INT	% OUT
					(Cp)Fe(Bz) (**2**, d^7)							
21a′	0	−0.131		16					38		28	20
13a″	1	−0.867		66		14			6		9	4
20a′	0	−0.871		66		14			6		9	4
19a′	2	−3.378	1	85	1			2			9	
12a″	2	−3.948		72		2			10		15	
18a′	2	−3.983		72		2			10		15	
11a″	2	−5.213	2	17		43			1		35	
17a′	2	−5.234	2	17		43			1		36	
16a′	2	−6.504	2	10		1			53		33	
10a″	2	−6.648		1				62		12	22	2
9a″	2	−6.683	2	10					53		33	
15a′	2	−8.146	4	1		43			18		30	3
					[(Cp)Fe(Bz)]⁺ (**1**, d^6)							
14a″	0	−0.912		13					55		30	2
21a′	0	−1.123		12					45		33	9
20a′	0	−2.058		59		18			9		11	2
13a″	0	−2.077		60		18			8		11	2
19a′	2	−5.005	1	86	1			1			9	
12a″	2	−5.515		77		3			8		12	
18a′	2	−5.562		78		3			7		12	
17a′	2	−6.381	3	18		41			4		34	
11a″	2	−6.404	3	19		41			3		33	
16a′	2	−7.456	2	16		3			50		29	
10a″	2	−7.500		2			1	61		13	22	
9a″	2	−7.650	2	14		2			52		30	
15a′	2	−9.034	5	1		41			22		29	2

[a] The analysis of the charge in the atomic spheres is made according to angular momentum contributions.

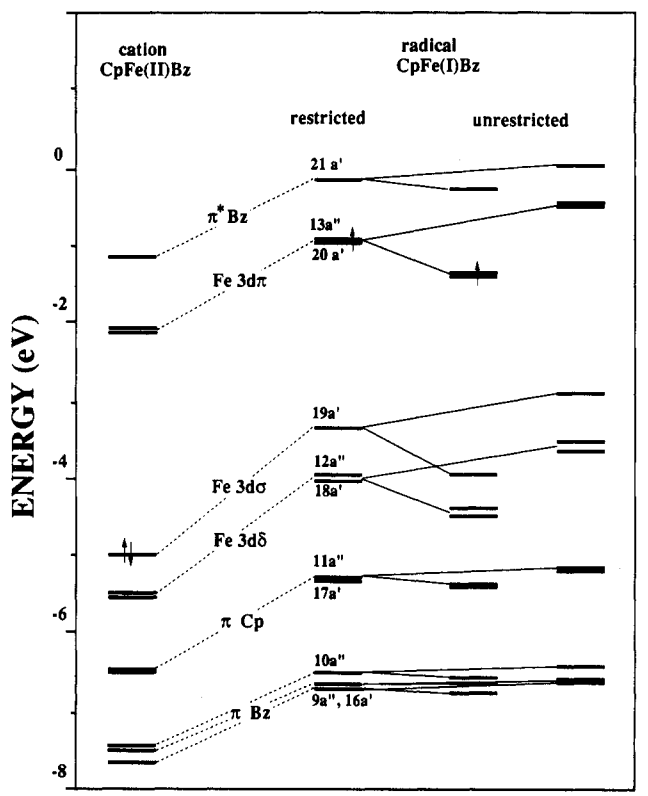

Figure 1. SCF SW-Xα upper energy levels for $[(Cp)Fe^{II}(Bz)]^+$ (**1**) and $(Cp)Fe^{I}(Bz)$ (**2**). The levels described as Fe 3d, π-Cp, and π-Bz are indicated. The occupation of the highest filled or partially filled orbital is shown.

in the mixed sandwich **2**, since the paired MO's (18a′, 12a″) of predominantly Fe 3dδ character (x^2-y^2, xy) are clearly bonding (Figure 2c) through an in-phase combination with π*-MO's $1e_{2u}$ and $1e''_2$ of C_6H_6 and C_5H_5, respectively (see Scheme III). This *δ back-donation* takes place mainly on the Bz ring (Bz 10% and Cp 2% of the MO character)

Scheme III

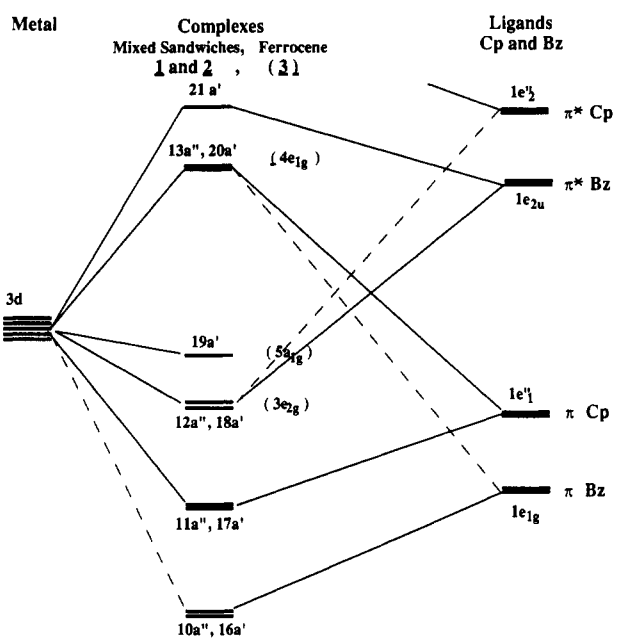

because the $1e_{2u}$ π*-MO is closer in energy to the Fe 3d atomic level. Besides, the first unoccupied 21a′ MO of the complex, which belongs to the antibonding partners, mainly corresponds to the destabilized $1e_{2u}$ π*-MO Bz orbital.

Nevertheless, in the radical (d^7) **2**, the Fe 3dπ orbital is partially occupied, which leads, in addition, to a π *back-donation* from the metal. The paired (20a′, 13a″) MO's, mainly exhibiting Fe 3dπ character, are obviously the antibonding partners (Scheme III and Figure 2b) of the bonding π-ligand orbitals (17a′, 11a″) discussed above, so it is not surprising that antibonding π *back-donation* also occurs mainly through the Cp ligand MO's. Nevertheless, owing to the half-occupation of only one of these paired

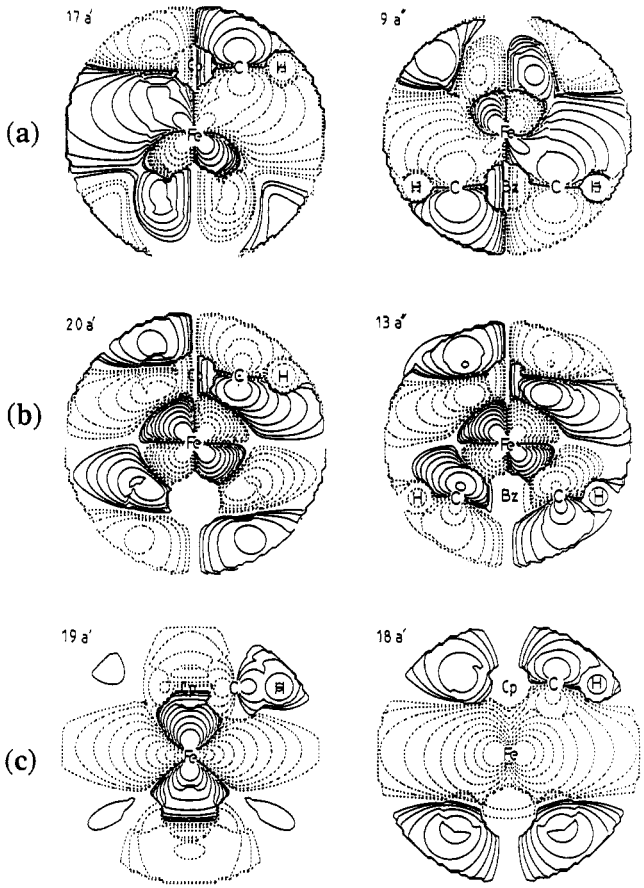

Figure 2. Contour maps of some MO's exhibiting important metal–ligand bonding and antibonding characteristics.

MO's, the 13a″ MO accomodating one electron, the antibonding π back-donation does not counterbalance the bonding π-ligand-to-metal charge donation.

Finally, the 19a′ MO (Fe $3d(z^2)$) is strongly localized within the metal sphere (85%; Figure 2c), which underlines its very weak contribution to the metal–ligand interactions.

c. 4s and 4p Bonding. Examination of Table I shows that Fe 4s and Fe 4d orbitals play a substantial role in the bonding mechanism of the complex, the major part of the 4s and 4p population being due to transferred electrons from the ligand π-orbitals.

Actually, all these bonding charge transfers are summarized in the electronic configuration deduced for the metal from the summation of Fe contributions to valence MO's:

$$Fe3d^{6.69}\ (3d\delta^{2.95}\ 3d\sigma^{1.77}\ 3d\pi^{1.96})\ 4s^{0.26}\ 4p^{0.40}$$

which leads to a gross charge in the metal sphere of +0.65, confirming that the complex may be formally considered as $3d^7$.

(ii) The Mixed [(Cp)Fe(Bz)]$^+$ Cation 1. For this cation, the sequence of MO's with predominantly metal 3d character is also

$$18a', 12a''\ (3d\delta^4) < 19a'\ (3d\sigma^2) \ll 20a', 13a''\ (3d\pi^0)$$

As a primary consequence of the ionization of **2**, Figure 1 shows an overall stabilization of the energy levels. Since no changes in the ordering are observed, the large energy stabilization is noteworthy for the Fe $3d\sigma$ and Fe $3d\delta$ orbitals, with respect to the Fe $3d\pi$ and π-ligand MO's, which implies a reorganization of the metal–ligand bonding. Indeed, in spite of the oxidation, the metal configuration in the cation **1** is very similar to that in the radical **2**:

$$Fe\ 3d^{6.69}\ (3d\delta^{3.21}\ 3d\sigma^{1.82}\ 3d\pi^{1.66})\ 4s^{0.29}\ 4p^{0.45}$$

In other words, the electronic structure of the cation is very different from that obtained by removing an electron from the Fe $3d\pi$ orbital of the radical and by keeping all the orbitals frozen. This minor difference in the electronic configuration of the metal constitutes an important modification of the electronic structure (i.e. in the nature of metal–ligand bonds) of the two complexes of the redox system. A large electron relaxation occurs to compensate for the loss of electrons around the metal upon ionization: through an increased π charge transfer from ligands to the metal $3d\pi$ orbitals, especially from the Bz ring, the metal retrieves electrons; conversely, through a decrease of π back-bonding from the Fe $3d\delta$ back-donation to the π^* ligand MO's, the metal gives less electrons back to the ligands. As seen in Table I, this is expressed, on the one hand, by a significant increase in the metal character of the π-ligand MO's with a simultaneous reduction in the antibonding Fe $3d\pi$ MO and, on the other hand, by a lessening of the ligand character in the Fe $3d\delta$ orbitals of the cation.

(iii) Mixed Complexes and Metallocenes: Comparison of Bonding Properties. We now move to a comprehensive study of the effect of the ligand (Cp versus Bz) and the effect of the electronic configuration of the metal on the bonding properties of the present complexes **1–6**. The general pattern of the upper valence MO's of metallocenes is

$$e_{1g}(\pi\text{-Cp}) < e_{1u}(\pi\text{-Cp}) < e_{2g}(\text{Fe } 3d) \approx a_{1g}(\text{Fe } 3d) < e^*_{1g}(\text{Fe } 3d)$$

In Table II we present the charge distribution of the significant MO's of the metallocene series,[1h,i] and Figure 3 shows the Xα energy splitting of the metal 3d orbitals. In order to compare homogeneous results, values for ferrocene (**3**) in Table II are the results of our calculations performed with Xα parameters similar to those for mixed sandwiches, especially by introducing an empty sphere in the center of each Cp ring. The metal configuration calculated in ferrocene (**3**) is

$$Fe\ 3d^{6.78}\ (3d\delta^{3.32}\ 3d\sigma^{1.76}\ 3d\pi^{1.69})\ 4s^{0.29}\ 4p^{0.44}$$

In metallocenes, the important parameter which governs orbital interactions is the energy value of the atomic metal 3d level with respect to that of the π e''_1 and π^* e''_2 MO's (Scheme III) of the Cp ligands. Table II shows, as one goes from Fe to Ni, an increase of the metal character in the bonding e_{1g} orbital, which leads, in turn, to an increase in the covalent bonding interaction. Simultaneously, a decrease of the metal character in the antibonding e^*_{1g} MO is observed. These trends can be related to the lowering of the metal 3d orbital energy when going from Fe to Ni. On the other hand, it is seen in Figure 3 that, as one goes from compound **3** to **4** and **6**, the energy difference between the a_{1g} and e_{2g} levels decreases (0.53, 0.39, 0.25 eV). This is undoubtedly due to the decrease of $3d\delta$ metal–ligand interactions, which consequently reduces the amount of π back-bonding from the iron to the π^* framework of the Cp ligands. On the basis of the larger a_{1g}–e_{2g} energy gap, it appears that the π-back-bonding is greater in the mixed radical sandwich **2** than in ferrocene (**3**), which is expected from the π-back-bonding

Table II. Spin-Restricted SW-Xα Upper Valence Levels and Charge Distributions[a]

	$(Cp)_2Fe$ (3, d^6)				$(Cp)_2Co$ (4, d^7)				$[(Cp)_2Ni]^+$ (5, d^7)				$(Cp)_2Ni$ (6, d^8)			
level[b]	energy (eV)	% M d^c	% C π^d	% INT	energy (eV)	% M d^c	% C π^d	% INT	energy (eV)	% M d^c	% C π^d	% INT	energy (eV)	% M d^c	% C π^d	% INT
$4e_{1g}$	−2.02	61	24	10	−2.19	57	27	12	−3.90	37	41	20	−2.80	49	34	16
$5a_{1g}$	−4.85	84		11	−4.68	87		9	−6.61	93	1	6	−5.09	92		7
$3e_{2g}$	−5.38	82	5	12	−5.07	86	4	9	−6.87	93	1	5	−5.34	92	1	6

[a] The analysis of the charge in the atomic spheres is made according to angular momentum contributions. [b] The 4e1g level is unoccupied for 3; it is occupied with one electron in 4 and 5 and with two electrons in 6. [c] Metal d orbital character. [d] Cp p orbital character.

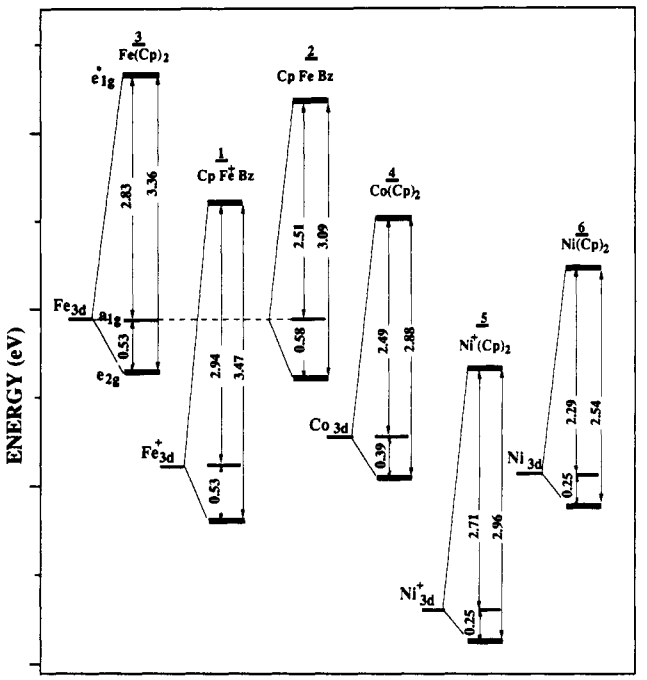

Figure 3. SCF SW-Xα 3d energy splittings. The energy levels have been displayed with respect to the nonbonding Fe 3d(z^2) energy levels of 2 and 3 which have been aligned.

character of the benzene ligand. Compounds 1 and 2 present an inverse trend to that reported above in metallocenes, since, as one goes from d^7 to d^6, we observe an increase of the π-ligand covalency and a decrease of the Fe 3dδ back-donation. However, as discussed above, this may be related to the overall stabilization of the levels with the cationic charge (Figure 1). Furthermore, the cationic effects are similar as one goes from nickelocene (6) to its cation 5. Although, in metallocene series, the charge distribution displays an increasing π-ligand → metal covalency, the global energy splitting between e^*_{1g} and e_{2g} levels is reduced on going also from 3 to 4 and 6. Actually this may be related to the increasing number of electrons in the antibonding e^*_{1g} MO as one goes from d^6 to d^7 and d^8, which, in turn, increases the metal–ligand distance and thereby decreases the overlap S between metal and ligand π orbitals.

Nevertheless, for a metal–ligand bonding mode described from a simple scheme of interaction between the metal and the ligand frontier molecular orbitals,[13] the perturbation theory predicts that the energetic stabilizations are proportional to $S^2/\Delta E$ with S and ΔE being respectively the overlapping and the energetic deviations between the interacting orbitals. Therefore, this qualitative discussion on the energy gaps of Figure 3, mainly based on the changes of the energy deviation ΔE between the metal and ligand orbitals (either one moving with respect to the other or vice versa) remains rough. Thus, in order to have some more quantitative information on the comparison between the two sets of ligands, we have reported in Table III the amount of the electronic charge transferred from each type of ligand to metal and also the amount of metal to ligand charge donation.

(13) (a) Fukui, K. *Fortschr. Chem. Forsch.* **1970**, *15*, 1. Epiotis, N. O.; Yates, R. L. *J. Am. Chem. Soc.* **1976**, *98*, 461.

Table III. Calculated SW-Xα Metal → Ligand and Ligand → Metal Electron Transfers

	$Fe(Cp)_2$ (3, d^6)	$Co(Cp)_3$ (4, d^7)	$[Ni(Cp)_2]^+$ (5, d^7)	$Ni(Cp)_2$ (6, d^8)
π-ligand donation (Cp)	+0.83	+0.90	+1.32	+1.10
3dδ back-donation	−0.36	−0.28	−0.14	−0.16
3dπ back-donation	0.0	−0.22	−0.32	−0.51
total	+0.47	+0.40	+0.86	+0.43

	$[(Cp)Fe(Bz)]^+$ (1, d^6)		(Cp)Fe(Bz) (2, d^7)	
	Cp	Bz	Cp	Bz
π-ligand donation	+0.90	+0.82	+0.76	+0.60
3dδ back-donation	−0.24	−0.66	−0.19	−0.93
3dπ back-donation	0.0	0.0	−0.24	−0.10
total	+0.66	+0.16	+0.33	−0.43

It is seen that for 1 and 3 d^6 complexes the total amounts of these charge transfers are 0.94 e^- (0.47 × 2(Cp)) and 0.82 e^- (0.66 (Cp) + 0.16 (Bz)), respectively. One deduces then that the behavior of one Cp ligand is very different in both complexes, as it globally donates 0.47 e^- to the metal in ferrocene (3) and 0.66 e^- in the mixed cation 1. In the metallocene series the amount of Cp π donation shows a weak increase as one goes from 3 to 4 and 6, while the π back-bonding from 3dδ orbitals to π* ligand orbitals is reduced at the same time, which is expected by examination of the trends in bonding discussed above. The larger value (0.86 e^-) obtained for the nickelocene cation 5 may be related to the cationic effect, as may also be the very different behavior of the Cp ligand in mixed-sandwich complexes 1 and 2. It is then again evident that the oxidation of these complexes cannot be be simply described by removing one 3d electron: in the cation the ligands act as better π-electron donors when the metal has less π back-bonding to the π* ligand MO's. The comparison of the d^7 cobaltocene (4) and d^7 mixed sandwich 2 shows a similar donation of the Cp ring (i.e. 0.40 e^- for 4 and 0.33 e^- for 2). However, it must be noted that the Bz ligand behaves very differently from the Cp ligand, its electron-acceptor character of 0.43 e^- in the mixed complex 2 being proof that much better π back-bonding occurs to this ligand.

(iv) Spin-Polarization Effects. Finally, it is interesting to examine the effect of spin polarization on the charge distribution of these d^7 complexes (Cp)Fe(Bz) (2) and $Co(Cp)_2$ (4). It is well-known in quantum chemistry that open-shell systems, in which the electrons do not accommodate all the orbitals by pairs, cannot be dealt with using the same one-electron models as for closed-

Table IV. Unrestricted SW-Xα Charge Distributions and Radial Integrals of the Important Upper Levels

	(Cp)Fe(Bz) (2)				$Co(Cp)_2$ (4)			
orbitals	% $\rho^{\uparrow}$	% $\rho^{\downarrow}$	$\langle r^{-3}\rangle^{\uparrow}$ (au)	$\langle r^{-3}\rangle^{\downarrow}$ (au)	% $\rho^{\uparrow}$	% $\rho^{\downarrow}$	$\langle r^{-3}\rangle^{\uparrow}$ (au)	$\langle r^{-3}\rangle^{\downarrow}$ (au)
3d π	62.4		6.01		51.4		7.16	
3d σ	86.4	84.4	5.09	4.93	87.7	85.7	6.07	5.93
3d δ	74.6	64.6	4.91	4.68	87.7	84.4	5.90	5.74
	75.6	64.3	4.90	4.66				
π e_1 (Cp)	13.6	9.0	4.16	3.68	43.6	35.3	5.36	5.02
	22.1	17.9	4.56	4.11				
π e_1 (Bz)	12.8	8.8	4.09	3.62				
	22.5	18.2	4.56	4.13				

Table V. Unrestricted SW-Xα Metal 3d Populations and 3d Spin Densities

	3d $\delta^{\uparrow}$	3d $\delta^{\uparrow-\downarrow}$	3d $\delta^{\downarrow}$	3d $\sigma^{\uparrow}$	3d $\sigma^{\uparrow-\downarrow}$	3d $\sigma^{\downarrow}$	3d $\pi^{\uparrow}$	3d $\pi^{\uparrow-\downarrow}$	3d $\pi_{\downarrow}$
(Cp)Fe(Bz) (2)	1.59	(0.20)	1.39	0.90	(0.02)	0.88	1.35	(0.78)	0.57
$Co(Cp)_2$ (4)	1.78	(0.07)	1.71	0.91	(0.02)	0.89	1.51	(0.70)	0.81

shell compounds.[14] The most common treatment of such systems is the so-called unrestricted Hartree–Fock method (UHF), or spin-polarized (SP) model for density functional methodologies such as MS–Xα. In this approach, different spatial orbitals are assigned to electrons with different spins, which leads to two sets of MO's obtained by solving the one-electron equations for spin-up and spin-down electrons, respectively. The advantage of performing SP calculations for radicals is that they lead generally to a lower total energy than their non-spin-polarized (NSP) counterparts; i.e., the corresponding wave functions are better approximations to the exact solution.

In Table IV, we have collected, for the d^7 **2** and **4** radicals, the SP SW–Xα charge distribution on the metal ρ_{Fe} as well as radial integrals $\langle r^{-3}\rangle_{3d}$ which provide, through the orbital radial functions, information regarding spin polarization, degree of delocalization, and bonding. In all the MO's exhibiting some metal 3d character, both ρ_{Fe} and $\langle r^{-3}\rangle_{3d}$ are larger for spin-up levels with respect to those values for their spin-down counterparts, which indicates a greater delocalization of the spin-down electrons and a contraction of the spin-up charge density toward the metal. Another conclusion which emerges from Table IV is that $\langle r^{-3}\rangle_{3d}$ values exhibit significant variations as a function of orbital energy. Orbitals with higher energies generally have larger values of $\langle r^{-3}\rangle_{3d}$ than the lower-lying orbitals. This is due to the well-known trend of antibonding orbitals to place more charge near the metal nucleus, which leads to larger values of $\langle r^{-3}\rangle_{3d}$, in contrast with bonding MO's which tend to expand their charge toward the ligands, thereby reducing the $\langle r^{-3}\rangle_{3d}$ values. All this discussion concerning charge and radial integrals is obviously confirmed in Figure 1. Though the sequence of spin-up and spin-down orbitals of **2** is respectively unchanged compared to NSP calculations, the orbitals with predominant Fe 3d character exhibit, nevertheless, the largest splitting between their spin-up and spin-down components, which leads to some interesting trends. Thus, the energy difference between spin-up Fe 3dπ (13a″, 20a′) and π-Cp (11a″, 17a′) MO's tends to decrease, thereby increasing π-Fe–ligand covalency. The corresponding metal and ligand characters displayed in Table IV are obviously in agreement with one another. The opposite trends are observed in mainly Fe 3dδ and empty π*-ligand orbitals: there is an increase of the Fe character in 3dδ spin-up orbitals with respect to the NSP ones. Obviously, electronic reorganization within spin-down orbitals is the inverse of that observed for spin-up MO's.

In the SP case, the metal electronic configuration obtained for **2** is

$$3d^{\uparrow 3.841}\ 3d^{\downarrow 2.825}\ (3d\delta^{\uparrow 1.587}\ 3d\delta^{\downarrow 1.385}\ 3d\sigma^{\uparrow 0.903}\ 3d\sigma^{\downarrow 0.878}\ 3d\pi^{\uparrow 1.351}\ 3d\pi^{\downarrow 0.562})\ 4s^{\uparrow 0.118}\ 4s^{\downarrow 0.114}\ 4p^{\uparrow 0.242}\ 4p^{\downarrow 0.189}$$

It should be noted that 3dδ electrons exhibit also a non-negligible exchange spin polarization: they lead to a spin density of 0.20 compared to a spin density of 0.78 for 3dπ electrons, for a total spin density of 1.02.

Examination of Table V shows that spin-polarization effects on 3dδ metal populations are 3 times smaller for **4** than for **2**, the other contributions being nearly equal. This is related to the fact that in **2** the 3dδ orbitals exhibit a greater interaction with the Bz ligand.

B. Electric Hyperfine Interactions (Mössbauer Parameters). Early works[1j,4a,b] have shown the ability of the Xα–SW wave functions to provide satisfactory interpretation of the electric and magnetic hyperfine interactions and to predict the spectroscopic properties of organometallics. Thus, we now turn our interest to the electric hyperfine interactions associated with the Fe nuclei of compounds **1–3**. The total energy of the electrostatic interaction between a nucleus, with the charge Ze, and surrounding charge may be split[15] into the two terms E_{IS} and E_Q.

The first term E_{IS} represents the *electric monopole interaction*, i.e., the electrostatic Coulomb interaction, between the nuclear charge Ze, which is spread over a finite volume, and electrons inside the nuclear region, s electrons having the ability to penetrate the nucleus. This causes a shift of the nuclear energy levels and gives rise to the isomer shift[15]

$$\Delta E_{IS} = (2\pi Ze^2/3)(\Delta|\Psi(0)|^2)(\Delta\langle r^2\rangle)$$

where $\Delta|\Psi(0)|^2$ and $\Delta\langle r^2\rangle$ correspond to the electronic and nuclear effects, respectively. Another convenient expression of the isomer shift is $\delta = \alpha\,\Delta|\Psi(0)|^2$.

Through $\Delta|\Psi(0)|^2$ the isomer shift measures the "s" electron density at the Fe nucleus arising from contributions of the electron density at the origin of the s orbitals: $|\Psi(0)|^2 = \sum_{ns}\rho_{ns}(0)$ with $\rho_{ns}(0) = N_{ns}|\phi_{ns}(0)|^2$, where N_{ns} is the number of electrons in the ϕ_{ns} orbital. Through the calibration constant α, which contains all the nuclear

(14) Hehre, W. J.; Radom, L.; Schleyer, P. v. R.; Pople, J. A. *Ab Initio Molecular Orbital Theory*; Wiley: New York, 1986.

(15) Gütlich, R.; Link, A.; Trautwein, A. X. *Mossbauer Spectroscopy and Transition Metal Chemistry*; Inorganic Chemistry Concepts 3; Springer-Verlag: Berlin, Heidelberg, New York, 1978.

Table VI. Restricted SW-Xα Contributions to the s-Electron Density at the Fe Nucleus

	(Cp)Fe(Bz) (**2**, d^7)	$Fe(Cp)_2$ (**3**, d^6)	[(Cp)Fe(Bz)]⁺ (**1**, d^6)
$\rho_{1s}(0)$ (au)	10 752.205	10 751.989	10 752.624
$\rho_{2s}(0)$ (au)	978.922	978.910	978.913
$\rho_{3s}(0)$ (au)	139.893	140.012	140.054
$\rho_{4s}(0)$ (au)	2.428	2.862	2.798
total $\rho_{ns}(0)$ (au)	11 873.448	11 873.773	11 874.389
exptl IS (mm/s)	0.74	0.53–0.65	0.45

constants, the isomer shift is related to the fractional charge radius $\delta R/R$ on excitation ($\alpha = C(\delta R)/R$). For the ^{57}Fe Mössbauer spectroscopy $\delta R/R$ is negative; therefore, an increase of the isomer shift in a series of Fe compounds indicates a decrease of the electron density at the Fe nucleus.

The Xα charge densities at the Fe nucleus of radical **2**, cation **1**, and ferrocene (**3**) are given in Table VI. We obtain a higher s-electron density for the d^6 complexes **1** and **3** as compared with that for the d^7 radical complex **2**, which is in agreement with their smaller experimental isomer shift. As one goes from the radical **1** to its cation **2**, the calculated s-electron density $\Delta|\Psi(0)|^2$ increases to $+0.941a_0^{-3}$, while the isomer shift ΔE_{IS} is reduced of −0.29 mm/s, which leads to the calibration constant $\alpha = -0.30a_0^3$ mm/s, in agreement with accurate determinations of this constant.[1f,16] The individual subshell contributions provide information on the bonding properties and metal valency. Indeed, the electronic mechanisms affecting ΔE_{IS} can be divided between the direct contributions arising from the 4s valence shell and the indirect contribution from 3d bonding which affects the s-electron distributions. Increasing the d-electron density increases the screening of the nuclear potential for s electrons, i.e., weaker attraction of the s-electron cloud by the nuclear charge, thereby decreasing the s-electron density at the nucleus. We then notice that the valence 4s electrons play a substantial part in the difference between the s density of d^6 **1** and **3** and that of d^7 radical **2**. This can be related to the slight increase in the amount of 4s electrons. Moreover, in addition to an important core 1s contribution, we only note weak differences between 3s electron densities of the complexes with regard to those expected between formal Fe(II) and Fe(I) ions. This supports the fact that Fe 3s electrons in the complexes undergo similar shielding efficiency from 3d electrons, i.e. the relaxation charge transfer leads to almost the same effective 3d charge for the nominal ions Fe(II) and Fe(I). In other words, the withdrawal of 3d electrons on oxidation is compensated by the electrons gained from a better π-ligand donation and a lesser π back-bonding.

The second term E_Q concerns the *electric quadrupole interaction*. It splits degenerate nuclear energy levels and yields the quadrupole splitting ΔE_Q, which measures the interaction between the electric quadrupole moment of the nucleus eQ and the electric field gradient (EFG). For nuclei having nuclear states with spin quantum number $I > {}^1/_2$, the nuclear charge distribution deviates more or less from a spherical symmetry, and eQ is a measure of this deviation. As Q is constant for a given Mössbauer nuclide, changes in ΔE_Q, observed under constant experimental conditions, can only arises from changes in the EFG, which is produced by the asymmetry of the electron density around the nucleus. Therefore, through the EFG, ΔE_Q depends on the chemical environment of the metal, i.e. on symmetry, covalency, valency, temperature, etc.

In a zero magnetic field the quadrupole splitting is given by[15] $\Delta E_Q = {}^1/_2 eQV_{zz}(1 + \eta^2/3)^{1/2}$, where Q is the quadrupole moment of the iron nucleus, V_{zz} is the principal component of the EFG tensor with $|V_{zz}| > |V_{yy}| > |V_{xx}|$ and $V_{zz} + V_{yy} + V_{xx} = 0$. The asymmetry parameter η is defined as $(V_{yy} - V_{xx})/V_{zz}$. The components of the EFG tensor are evaluated as the sum, over all the valence electrons, of the products of a radial integral $\langle r^{-3}\rangle$ times the angular contribution $\langle \sigma_{lm}\rangle$: $V_{zz} = -e\sum\langle \sigma_{lm}\rangle\langle r^{-3}\rangle$. The components of the EFG as well as the quadrupole parameters are gathered in Table VII. With regard to the 3d contributions, it is worth considering the substantial inverted effect of 4p electrons. We observe that the electronic oxidation occurring when going from the Fe(I) radical **2** to the Fe(II) **1** cation is associated with a drastic increase of V_{zz}, i.e. from 0.066 to 1.295, respectively. These values give rise to quadrupole splittings with both sign and magnitude in agreement with the experimental results obtained at room temperature. In the radical, V_{zz} increases significantly and its sign changes if we consider only the 13a″ MO as being occupied at low temperature. This is also in agreement with the temperature dependence of both ΔE_Q and the sign of the EFG. However, the calculated ΔE_Q is overestimated, which may suggest a partial occupation of the 13a″ and 20a′ MO's even at low temperature.

Of particular interest is the comparison between the results for the cation and those deduced from the fully occupied levels up to the 19a″ MO of the radical. V_{zz} is the sum of individual contributions which can be of opposite signs (angular factors) and which not only depend on the charge distribution of the orbitals but also on the $\langle r^{-3}\rangle$ values. Then a deeper examination shows that if the total V_{zz} increases by only about 12% from Fe(I) to Fe(II), the π contributions differ by as much as 36%, which underlines again the electronic reorganization induced by oxidation.

Thus, the d^7 Fe(I) radical complex **2** cannot be viewed as a simple sum of the d^6 Fe(II) complex **1** and one electron.

C. Ionization and Electronic Excitation Energies. The Xα ionization energies of the radical complex **2** and the UV photoelectron (PE) results for related compounds are presented in Table VIII, whereas the electronic excitation energies of **1** and **2** are reported together with optical absorption data in Table IX. For a detailed assignment of either the PE spectrum or absorption bands, it may be useful to compare the PE spectrum of the neutral complex with the electronic absorption spectrum of its cation. Indeed, comparable information on the ordering and separation of ion states can be obtained, within a certain energy range, from the different Franck–Condon envelopes of the two processes.[5] Another procedure, allowing us to rationalize these data, consists of comparing them with those reported for isoelectronic compounds such as cobaltocene and its cation.

From changes in peak intensity between the He I and He II spectra as well as from their studies on cobaltocene, Green et al.[5] assigned the four lowest PE bands (A–D) of the radical complex to the ionization of Fe 3d electrons and the other two well-resolved PE bands (E, F) to ligand ring electrons. As seen in Table VIII, this interpretation is in agreement with our calculated values. Whereas the

(16) (a) Duff, K. J. *Phys. Rev.* **1974**, *B9*, 66. (b) Nieuwpoort, W. C.; Post, D.; Van Duijnen, P. Th. *Phys. Rev.* **1978**, *B17*, 91.

Table VII. Detailed SW-Xα Contributions to the Electron Field Gradient at the Fe Nucleus and Comparison with Experimental Parameters

	radical (Cp)Fe(Bz) (**2**, d^7)			cation $[(Cp)Fe(Bz)]^+$ (**1**, d^6)		
orbital	V_{xx}	V_{yy}	V_{zz}	V_{xx}	V_{yy}	V_{zz}
			Filled Orbitals			
$3d\sigma(z^2)$	1.1935	1.1935	−2.3871	1.2415	1.2415	−2.4830
$3d\delta(x^2-y^2, xy)$	−1.9095	−1.9095	3.8189	−2.1306	−2.1306	4.2644
$3d\pi(xz)$	0.6506	−0.3253	−0.3253	0.8924	−0.4462	−0.4462
$3d\pi(yz)$	−0.3190	0.6381	−0.3190	−0.4325	0.8650	−0.4325
total 3d	−0.787	−0.786	1.573	−0.858	−0.941	1.799
4p(z)	0.3638	0.3638	−0.7277	0.4201	0.4201	−0.8402
4p(y)	0.2620	−0.5239	−0.2620	0.2942	−0.5884	−0.2942
4p(x)	−0.5154	0.2577	0.2577	−0.5879	0.2940	0.2940
total 4p	0.207	0.207	−0.414	0.252	0.252	−0.504
total 3d + 4p	−0.580	−0.579	1.159	−0.606	−0.689	1.295
			Half-Filled Orbitals			
13a″	−1.093	2.186	−1.093			
20a′	2.186	−1.093	−1.093			
mean (13a″ + 20a′)	0.547	0.546	−1.093			
Total All Electrons						
low temp (13a″)	*−1.673*	1.607	0.066			
high temp (13a″ + 20a′)	−0.033	−0.033	*0.066*			

	SW-Xα EFG params			exptl EFG params		
	V_{zz}	ΔE_Q	η	sign (EFG)	ΔE_Q	η
cation $[(Cp)Fe(Bz)]^+$ (**1**)	1.295	1.97	0.06	>0	1.89	≅0
radical (Cp)Fe(Bz) (**2**)						
low temp	−1.673	−2.86	0.9	<0	1.5	
high temp	0.066	0.10	0	>0	0.38	0

Table VIII. Comparison of SW-Xα and Experimental (UV Photoelectron Spectroscopy) Ionization Energies

		energy (eV)					
orbital	character	**2**[a]	$(C_5Me_5)Fe^I(C_6Me_6)$[b]	$(Cp)Fe^I(C_6Me_6)$[b]	**4**[b]	assignt	band
13a″, 20a′	Fe $3d\pi$	3.56	3.95, 4.21	4.68	5.55	A^1	A
19a′	Fe $3d\sigma$	6.17	5.74	6.19	7.15	$E^1 + E^2$	B
12a″, 18a′	Fe $3d\delta$	6.70, 6.74	6.32	6.92	7.60	$E^1 + E^1$	C
			6.64	7.18	7.99	$E^2 + E^1$	D
11a″, 17a′	Cp 2p	7.78, 7.80	(7.20), 7.71	7.89	8.72	e^1 Cp	E
9a″, 16a′	Bz 2p	8.70, 8.91	8.58	8.79, 9.06	9.92	e^1 Bz	F
10a″	Bz 2p	9.11					
15a′	Cp, Bz 2p	10.55					
14a′, 8a″	Cp 2p, H	10.81	10.2			rings	
13a′	Bz 2p, H	11.02					
7a″, 12a′	Cp 2p, H	11.24					
11a″	Cp, Bz 2p	11.50					
10a′	Bz 2p, H	11.61					
6a″	Bz 2s, 2p	12.02					
5a″	Bz 2p, H	13.11	13.0			rings	
9a′	Cp 2s, 2p	14.49					

[a] Theoretical value (SW-Xα). [b] Experimental value.

Table IX. Comparison of SW-Xα and Experimental Electronic Transition Energies (eV)

		theor SW-Xα data		exptl optical data				
transition	character	**2**	**1**	**2**	**1**	$CpFe^{II}C_6Me_6$	$[Co(Cp)_2]^+$	assignt
20a′ → 21a′	Fe → Bz	0.9 (1.3)[a]		1.7				CT (M → L)[b]
							2.68	E
19a′ → 20a′	d–d	2.58 (2.62)	2.95		2.74	2.71	3.00	E
18a′ → 20a′	d–d	3.22 (3.13)	3.60		3.24	3.06	3.26	E
					3.96	3.82	4.12	E
17a′ → 20a′	Cp → Fe	4.59 (4.20)	4.45		4.73	4.67	4.69	CT (L → M)
16a′ → 20a′	Bz → Fe	6.05 (5.64)	5.67		5.17	6.06		CT (L → M)

[a] Unrestricted values. [b] CT = charge transfer.

lowest PE band (A) can safely be assigned to the $1A^1$ state, originating from ionization of the Fe $3d\pi$ antibonding orbitals, the nature of the PE B–D bands is much more controversial. Undoubtedly they are due to ionization of either Fe $3d\delta$ or $3d\sigma$ electrons, but the metal configurations $3d\delta^3\ 3d\sigma^2\ 3d\pi^1$ and $3d\delta^4\ 3d\sigma^1$ give rise to a complex multiplet structure, making it difficult to clearly assign these bands by the traditional methods of quantum chemistry. Our purpose is not to solve this problem, and our contention is simply that the predicted values 6.17 and 6.70 eV for ionization of $3d\delta$ and $3d\sigma$ orbitals, respectively, is consistent with the observed values. Moreover, the ionization energies of MO's with predominantly ligand character compare well with the two PE

bands E and F. The peak E is primarily due to the Cp ring ionization, while the peak F is mainly of Bz character.

The energy deviations between the first calculated ionization energy (A) and the first calculated ligand e_1 ionization energy (4.24 eV (Cp) and 5.14 eV (Bz)) of the radical can be compared with the first Xα ligand-to-metal charge-transfer transitions of the cation lying at 4.45 eV (Cp) and 5.67 eV (Bz), respectively. It is seen that the two calculations lead to a consistent energy difference between metal 3d and Cp vs Bz ligand orbitals. Such an agreement is not observed for the position of the corresponding experimental PE and UV bands, as they exhibit a discrepancy of 1 eV. In order to ensure consistency of these experimental data, Green et al.[5] assume that no adiabatic transition is observed in the PE band of the radical or that no Franck–Condon transition is observed in the ion, or both. As the calculated shift between vertical ionization and absorption energies is smaller, we are tempted to suggest that other effects may play a substantial role, such as the influence of solvent on absorption band position or orbital relaxation occuring during ionization and excitation.

Let us turn now to the electric absorption spectra. In the d^7 radical complexes a broad absorption band of low intensity is observed near 700 nm in the visible region. This is in agreement with our prediction of a symmetry-forbidden $e_{1g}(13a'', 20a') \rightarrow e_{2g}(21a', 14a'')$ Fe → ligand (Bz) charge-transfer transition in this energy range. It is interesting to note that the introduction of spin-polarization effects leads to a better agreement with experiment. As mentioned above, this is due to a greater splitting of spin components of the Fe 3d orbitals as compared with that for ligand ones. It should be added that specific permethylations of the Cp and arene ligands allows an assignment of this band.[6] Though they represent average values of several configurations arising from multiplet structure, the calculated transition between predominantly metal 3d orbitals are also in good agreement with experimental values. As compared with the d–d transitions of the radical, those calculated for the cation are shifted toward higher energies. Actually, this is an expected trend when the oxidation state of metal increases (i.e. the ligand field splitting of the metal orbitals enlarges with increasing oxidation number). Finally, the very strong bands in the absorption spectrum of the cation may be undoubtedly assigned to ligand-to-metal charge-transfer transitions allowed by both the Laporte and symmetry selection rules (i.e., $e_{1g}(17a', 12a'') \rightarrow e_{1g}(13a'', 20a')$ (Cp → Fe) and $e_{1g}(15a', 10a'') \rightarrow e_{1g}(13a'', 20a')$ (Bz → Fe).

IV. Conclusions

The present Xα calculations provide a detailed study of the electronic structure of the radical d^7 mixed sandwich complex CpFeBz and of its cation. These results, combined with further information from previous Xα investigations on metallocenes, lead to a comprehensive study of the ligand and electron-count effects on chemical bonding within these two complementary series of organometallic complexes.

In this work it is shown that the Cp and the Bz ligands behave differently as far as 3dδ back-bonding is concerned. The empty π^* orbitals of Bz, fairly close to 3d metal orbitals, allow a better back-donation of electrons from 3dδ metal orbitals to the ligand. Then in the mixed CpFeBz complex, the global electron-acceptor (+0.43 e^-) character of the Bz ligand acts in opposition to the electron-donor (–0.33 e^-) character of the Cp ligand. In the metallocene series this electron-donor character is appreciably increased. Upon ionization the effective charges of the nominal ions (i.e. Fe^+ and Fe^{2+} in mixed complexes or Ni^+ and Ni^{2+} in metallocenes) seem approximately unchanged, the largest difference in electron density being observed on the ligand rings. The withdrawal of 3d metal electrons on oxidation is then compensated by the electrons gained from a better π donation of the ligands and a reduction of the π back-bonding.

Confirmation of these trends is obtained by considering the analysis of the spin-polarization effects and the study of the electric hyperfine interactions. Then the spin polarization induces a 3dδ spin density, which is 3 times larger for the mixed radical CpFeBz (greater interaction between 3dδ orbitals and π^* Bz orbitals) with respect to that for cobaltocene. The similar Fe 3s contributions to the s-electron density at the Fe nucleus for both the radical and cation suggest similar shielding efficiencies from 3d electrons, which gives support to near-identical effective 3d charges for the nominal Fe^+ and Fe^{2+} ions.

Finally, a good agreement is obtained between theoretical electric hyperfine parameters and experimental results of Mössbauer spectroscopy. Similarly, both MS-Xα ionization and electronic excitation energies compare well with photoelectron and UV–visible absorption data.

Acknowledgment. This work has been supported by the Swiss National Science Foundation (Project 20-29856.90).

OM9200316